Hindawi Publishing Corporation
International Journal of Photoenergy
Volume 2011, Article ID 234931, 7 pages
doi:10.1155/2011/234931

Research Article

Influence of Titania Dispersivity on the Conversion Efficiency of Dye-Sensitized Solar Cells

Yasuhiro Yamamoto,[1,2] Yukihiro Aoyama,[1] Sumiyo Shimizu,[1] Junya Kano,[2] Fumio Saito,[2] and Seigo Ito[3]

[1] *Mikuni Color Ltd., 101 Kokubunji, Mikunino-cho, Himeji, Hyogo 671-0234, Japan*
[2] *Graduate School of Environmental Studies, Tohoku University, 2-1-1 Katahira, Aoba-ku, Sendai 980-8577, Japan*
[3] *Department of Electrical Engineering and Computer Sciences, Graduate School of Engineering, University of Hyogo, 2167 Shosya, Himeji, Hyogo 671-2280, Japan*

Correspondence should be addressed to Yasuhiro Yamamoto, yamamoto@mikuni-color.co.jp

Received 11 July 2011; Accepted 25 September 2011

Academic Editor: Roel van De Krol

Titania powder (P25) was dispersed by bead-milling breakdown method, and the dispersivity of TiO_2 was controlled by adjusting the mean secondary TiO_2 particle size to 45, 56, and 75 nm by changing the dispersion solvent blend ratio of ethanol and terpineol. The transparency of the coated layer increased when the particle size of TiO_2 aggregates became smaller than 100 nm. Although the transparency was significantly different according to differences in the size of nanocrystallyne-TiO_2 aggregates, the resulting photovoltaic (PV) effect of a dye-sensitized solar cell (DSSC) was not significantly different between the different aggregate sizes. A double layer structure (transparent TiO_2 layer/opaque TiO_2 layer) was adopted to improve the PV effect, which resulted in an improvement of the photocurrent and conversion efficiency of 13.2% and 11.1%, respectively, from that for the DSSCs with single-layered TiO_2 electrodes.

1. Introduction

Energy requirements throughout the world are primarily dependent on fossil fuel resources in the earth. In addition, various problems have occurred in a present global environment due to the global warming issue associated with carbon dioxide emissions from fossil fuel usage. Various problems include the recently unusual weather, depletion of the ozone layer, and sea level rise due to the greenhouse effect. Such problems are threatening the current status quo. In addition, fossil fuels such as petroleum oil are a limited resource that will be depleted and result in an oil crisis. Therefore, alternative energy sources, such as the sun, have been considered to change the dominant reliance on fossil fuels.

Solar cells are used to directly convert the energy from sunlight into electricity using the photovoltaic (PV) effect. Solar cells are generally classified into three types; silicon, metal compound, and organic-based systems. Organic-based solar cells are considered to be the next-generation solar cell, due to its ease of production. In addition, the production cost can be lowered, and it has features such as the ability for coloring and flexibility.

Dye-sensitized solar cells (DSSCs) [1] are one type of organic solar cell. The manufacturing cost of DSSCs is expected to be significantly lower than that of silicon-based solar cells. DSSCs employ TiO_2 as the semiconductor photoelectrode. The structure of the TiO_2 layer is nanocrystalline, which is important to improve the conversion efficiency, which is significantly influenced by the TiO_2 particle dispersivity. There are two chief methods for the production of fine TiO_2 particles (Figure 1). One is a build-up process, such as the hydrothermal method, and another is a breakdown method that uses a stirred media mill (such as a bead mill). TiO_2 particles produced by the buildup process are high purity and have a narrow particle size distribution because the TiO_2 particles can be gradually grown to optimum size without significant aggregation. However, the apparatus for

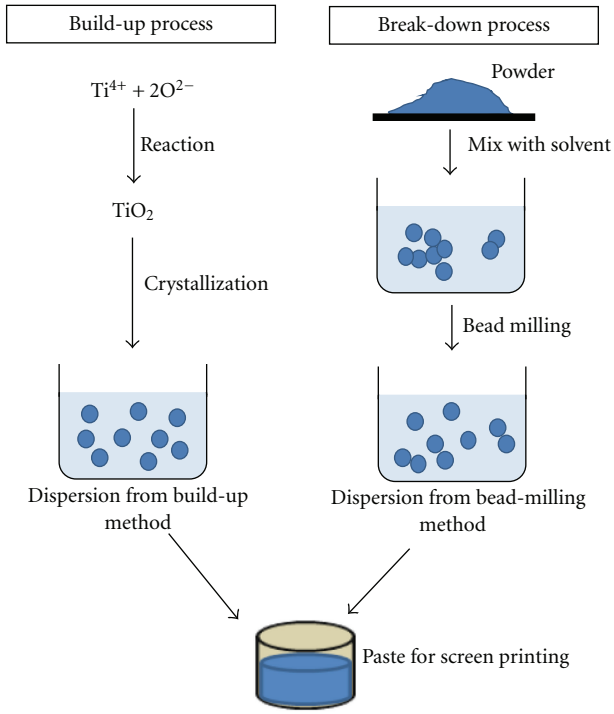

Figure 1: Conventional methods for the preparation of TiO_2 dispersions.

synthesis is expensive and the crystallization process is time consuming; therefore, it is not suitable for mass production. In contrast, the break-down method has advantages of low introduction costs of the manufacturing devices and the facile mass production, despite the broad particle-size distribution obtained compared with the hydrothermal method, which results from the imperfect dispersion of aggregate particles by bead collisions. However, the control of dispersivity has become possible through the use of computer simulation developed in recent years [2].

There have been many reports regarding the influence of factors such as the layer construction and type of the dye used on the conversion efficiency [3–6]. Although some reports have been published on DSSCs using TiO_2 aggregates synthesized by the hydrothermal method [7–10], no reports has been published about the particle size distribution using the bead-milling breakdown method, because control of the size distribution by bead milling is quite difficult. In this paper, the particle distribution of P25 titania powder was differed by dispersion control, and the influence of the physical properties of the TiO_2-coated layer on the PV conversion efficiency of a DSSC was investigated.

2. Experiment

2.1. Dispersion Experiment and Preparation of TiO_2 Paste. A paint shaker (Paint shaker, Asada Iron Works Co. Ltd., Japan) was employed as the milling system. The beads made of alumina were used and their diameter is 0.1 mm. The 250 cc container made from polyethylene was used. The bead filling ratio was set at the same volume of the dispersion material. The dispersion sample consisted of 15 wt% titania powder (Aeroxide TiO_2 P25, Degussa, Germany) and 4.5 wt% high-molecular-weight acrylic block copolymer dispersant in a mixture of ethanol and terpineol. Three different evaluation samples were prepared with their dispersivity adjusted by changing the mixing ratio of ethanol and terpineol at w/w = 9/1, 7/3, and 5/5, respectively. The dispersion time was 10 h. The particle size distribution was evaluated by a dynamic light scattering (Zetasizer Nano, Malvern Instruments Ltd., England) method. The crystallinity of TiO_2 was analyzed using X-ray diffraction (XRD; Mini Flex II, Rigaku, Japan).

2.2. Evaluation of TiO_2-Coated Layer. The TiO_2 layer used for evaluation of the PV conversion efficiency was made by screen-printing (230 mesh/inch) on fluorine-doped tin oxide (FTO) glass plate and heating at 500°C for 30 min. The coated layer was photographed and the morphology of the TiO_2 particles was observed using field emission scanning electron microscopy (FE-SEM; S-5200 Hitachi High-Technologies Corporation). The total transmittance and haze ratio of the TiO_2-coated layer were measured using ultraviolet-visible spectroscopy (UV-vis, Lambda 750, Perkin Elmer, USA).

2.3. Cell Fabrication Procedure

2.3.1. Materials. *cis*-Di(thiocyanato)-N, N′-bis (2,2′-bipyridyl-4-carboxylicacid-4′-tetra butyl ammonium carboxylate) ruthenium (II) (N-719; Solaronix SA), butyl methyl imidazolium iodide (BMII; Merk), 4-tert-butylpyridine (Aldrich), acetonitrile (Tokyo Chemical Industry), valeronitrile (Tokyo Chemical Industry), guanidinium thiocyanate (Aldrich), and H_2PtC_{l6} (Tokyo Chemical Industry) were used as received. H_2O was purified by distillation. $TiCl_4$ (Wako) was diluted with water to 2 M at 0°C as a stock solution, which was stored in a freezer and freshly diluted to 40 mM with water for each $TiCl_4$ treatment of the FTO-coated glass plates. Iodine (99.999%, Superpur, Merck) was used as received.

2.3.2. Preparation of TiO_2 Electrodes. Figure 2 shows an outline of the method for preparation of TiO_2 paste from the dispersion. The TiO_2 paste was prepared by mixing the dispersion and ethyl cellulose dissolved in ethanol and then removal of the ethanol from the mixture. To prepare the DSSC working electrodes, the FTO glass used as current collector (Solar 4 mm thickness, 10 ohm/sq, Nippon Sheet Glass, Japan) was cleaned in a detergent solution using an ultrasonic bath for 15 min and then rinsed with water and ethanol. After treatment in a UV-O_3 surface-cleaning system for 3 min the FTO glass plates were immersed into a 40 mM $TiCl_4$ aqueous solution at 70°C for 30 min, and then washed with water and ethanol. A layer of paste was screen printed (230 mesh/inch) on the FTO glass plates, which was then kept in a clean box for 3 min with ethanol to relax the paste film and reduce surface irregularities and then dried for 6 min at 125°C. This screen-printing procedure (coating,

storing, and drying) was repeated to adjust the thickness of the TiO_2 working electrode. The electrodes coated with TiO_2 paste were gradually heated under airflow at 325°C for 5 min, 375°C for 5 min, 450°C for 15 min, and 500°C for 15 min.

2.3.3. DSSC Assembly. After measuring the thickness of the layer, the TiO_2 layer was treated with 40 mM $TiCl_4$ solution, rinsed with water and ethanol, and sintered at 500°C for 30 min. After cooling to 80°C, the TiO_2 electrode was immersed into a 0.5 mM N-719 dye solution in a mixture of acetonitrile and tert-butyl alcohol (volume ratio: 1 : 1) and kept at room temperature for 20–24 h to complete the sensitizer uptake. A hole was drilled in the FTO glass (Nippon-Sheet Glass-Pilkington, 15 ohm/sq, 2.2 mm thick) counter electrode to insert the electrolyte into the cell after sealing. A perforated sheet was washed with H_2O and with a 0.1 M HCl solution in ethanol and cleaned by ultrasonication in an acetone bath for 10 min. After the removal of residual organic contaminants by heating in air for 15 min at 400°C, a Pt catalyst was deposited on the FTO glass by coating with a drop of H_2PtCl_6 solution (2 mg Pt in 1 mL ethanol) and repeating the heat treatment at 400°C for 15 min. The dye-covered TiO_2 electrode and Pt-counter electrode were assembled into a sandwich-type cell and sealed with a 25 mm thick hot-melt gasket made of the ionomer Surlyn 1702 (DuPont). The aperture of the Surlyn frame was 2 mm larger than that of the TiO_2 area, and its width was 1 mm. A drop of the electrolyte, a solution of 0.60 M BMII, 0.03 M I_2, 0.10 M guanidinium thiocyanate, and 0.50 M 4-tert-butylpyridine in a mixture of acetonitrile and valeronitrile (volume ratio: 85 : 15) was deposited through the hole in the back of the counter electrode. The electrolyte was introduced into the cell via vacuum backfilling. The cell was placed in a small vacuum chamber to remove internal air. Exposure of the cell to ambient pressure again causes the electrolyte to be driven into the cell. Finally, the hole was sealed using a hot-smelt ionomer film (Bynel 4164, 35 μm thick, Du-Pont) and a cover glass (0.1 mm thick).

2.4. Photovoltaic Measurement of DSSC. Photovoltaic measurements were conducted using an AM 1.5 solar simulator. The power of the simulated light was calibrated to be 100 mWcm^{-2} using a reference Si photodiode equipped with an IR-cutoff filter (Bunkou Keiki, Japan). Current density-voltage (*I-V*) curves were obtained by applying an external bias to the cell and measuring the generated photocurrent with a digital source meter. The voltage step and delay time of photocurrent were 10 mV and 40 ms, respectively.

Photo action spectra of dye-sensitized solar cells were measured using pyroelectric energy sensor (PE10-S, Ophir optronics Ltd., Israel) and bandpass filters from 400 nm to 800 nm.

3. Results and Discussion

The distribution of TiO_2 particles is shown in Figure 3. Each sample has different particle distributions due to the different ratios of ethanol and terpineol used, although the dispersion time used was the same. The mean particle sizes of TiO_2 in samples A, B, and C were 42.5, 56.9, and 73.4 nm, respectively. The primary particle size of P25 TiO_2 is 21 nm; therefore, approximately 2–4 primary particles were aggregated for sample A. The maximum particle size of sample A was around 100 nm. The mean particle size of sample B was 56.9 nm, and the TiO_2 particles were dispersed as aggregates composed of about 2–10 particles. The mean particle size of sample C was 73.4 nm, so that more than 10 TiO_2 particles are agglomerated and individual particles in sample C were largely agglomerated compared with sample A. Therefore, the dispersivity can be controlled according to the solvent blend ratio of ethanol and terpineol used in the dispersion.

Figure 4 shows XRD patterns for each TiO_2 sample. The peaks are confirmed as being almost the same position for all samples and the crystallinity was not degraded by the bead-milling process. The conversion efficiency of the DSSC may change with the crystallinity of TiO_2, so that TiO_2 particles

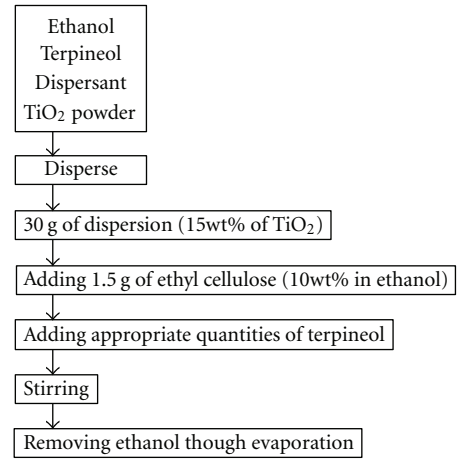

Figure 2: Method for the preparation of TiO_2 paste.

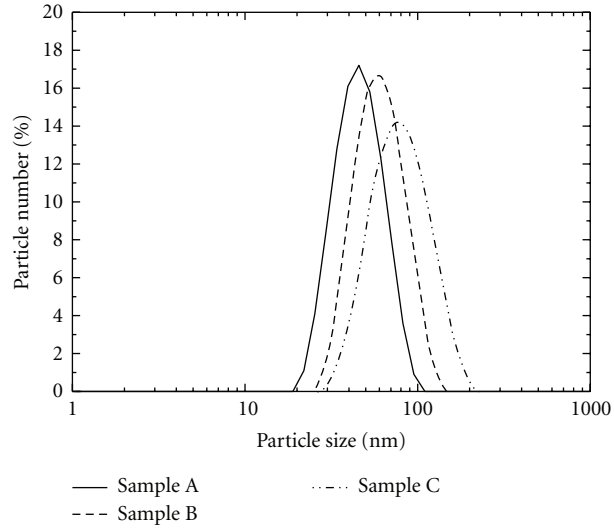

Figure 3: Particle size distribution of the TiO_2 dispersions.

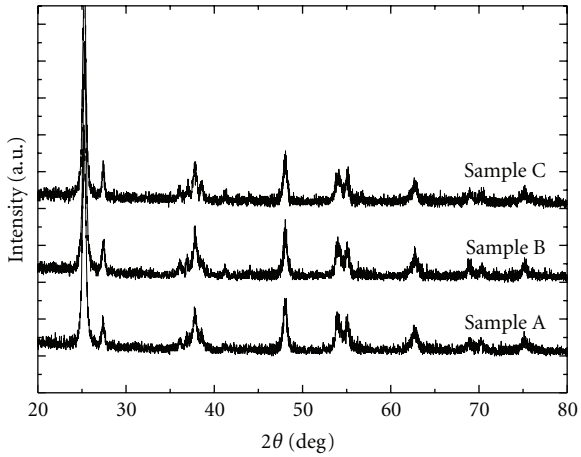

Figure 4: XRD patterns for TiO_2 dispersions with different dispersivity.

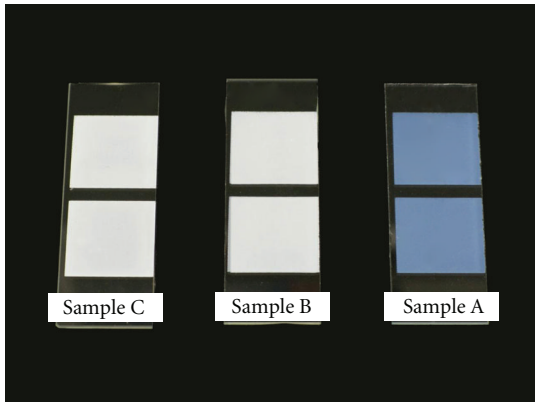

Figure 5: Optical photograph showing the appearance of 4 μm thick TiO_2-coated layers.

should be dispersed with consideration of the influence of bead-milling on the crystallinity.

The TiO_2 paste prepared by the method shown in Figure 2 was coated on the FTO glass plates by screen-printing, and then heated at 500°C for 30 min. Figure 5 shows photographs of the ca. 4 μm coated layers. The coated layer of sample A is translucent; however, samples B and C are opaque. These differences are due to the scattering of light. The scattering of light increases according to (1) to (4) [11–15], where D_{opt} is the particle size where the light scattering becomes the highest, λ is the wavelength of incident light, n_1 and n_2 are the refractive indices of the air and TiO_2 particles, respectively, and m is the ratio of refractive index, which is equal to n_2/n_1:

$$D_{opt1} = \frac{0.9\lambda(m^2+2)}{n_1\pi(m^2-1)}, \quad (1)$$

$$D_{opt2} = \frac{\lambda}{2(n_2-n_1)}, \quad (2)$$

$$D_{opt3} = \frac{\lambda(m^2+2)}{1.414n_1\pi(m^2-1)}, \quad (3)$$

$$D_{opt4} = \frac{2\lambda}{(n_2-n_1)}. \quad (4)$$

When the incident wavelength is assumed to be 400 nm, light scattering becomes the highest for TiO_2 particle sizes of 167, 114, 131, and 145 nm from (1), (2), (3), and (4), respectively. That is, the scattering of light increases with the increase in the number of particles over 100 nm. The coated layer of sample A was translucent because the particles in sample A were almost all less than 100 nm (from Figure 3). In contrast, the coated layers of samples B and C appeared white because they consisted of particles over 100 nm. Therefore, the coated layer became significantly opaque due to light scattering of particles with sizes greater than 100 nm present in the coated layer.

Figures 6(a) and 6(b) show the transmittance and haze ratio of the coated layers from UV-vis measurements as a function of wavelength. The transmittance of sample A was higher than those of samples B and C, which had almost comparable transparency. The haze ratio of sample A was lower than those of the other samples for all wavelengths in the visual light range. The haze ratios of samples B and C were almost 100% for wavelengths below 500 nm, due to the light scattering of these samples.

Figure 7 shows FE-SEM images of the morphologies of the coated layers. Each sample was made of P25 TiO_2 nanoparticles heated at 500°C for 30 min. The difference in the morphologies was attributed to the aggregation-size distribution. The pore size of the coated layer changes when the calcinations temperature is varied [7]; however, the samples were calcined under the same conditions. For sample A, the particles were well dispersed, so that the coated layer was flat and smooth. However, for samples B and C, many voids were clearly evident in the TiO_2 layer. The sizes of the voids in sample C were larger than that in sample B, due to the size of the TiO_2 aggregations (Figure 3). Although the primary particle size was the same, the voids between the TiO_2 aggregates influence the transmittance and haze ratio of the coated layer. It has been reported by previous report [16] that the void makes increasing of scatter light. When the mean particle size becomes large, the voids also may increase from Figure 7. Therefore, scatter light increases under the influence of the particle size and the void. The more a mean particle is large, the more scatter light increases, and then coated layer looks opaque.

Table 1 shows the PV properties of DSSCs prepared from TiO_2 dispersions. The mean particle size of sample A was small, so that the pore size of the coated layer was small. Therefore, the specific surface area of the coated layer was increased and much dye is adsorbed, so that the conversion efficiency increases. In contrast, samples B and C had many large voids in the coated layer, so that high conversion efficiency could not be expected. However, the conversion efficiencies and other PV properties of each of the samples were not significantly different, regardless of the mean particle size of the dispersion. The high transparency of the coated TiO_2 layer means that the incident light can pass through

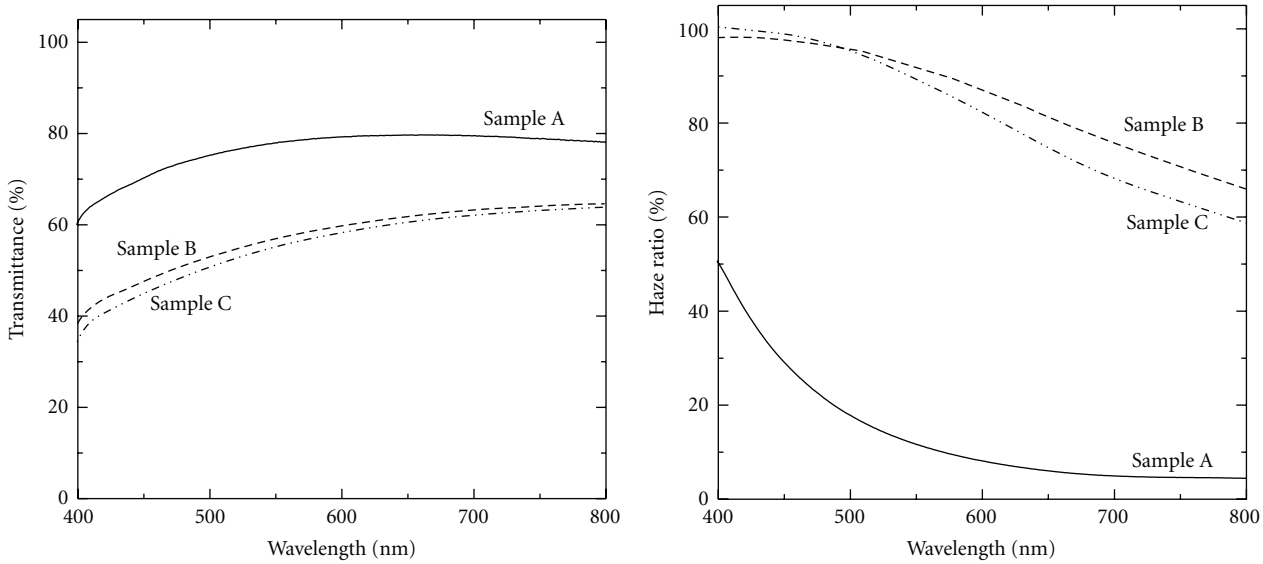

(a) Transmittance (b) Haze ratio

Figure 6: (a) Transmittance and (b) haze ratio for TiO_2-coated layers from UV-vis measurements.

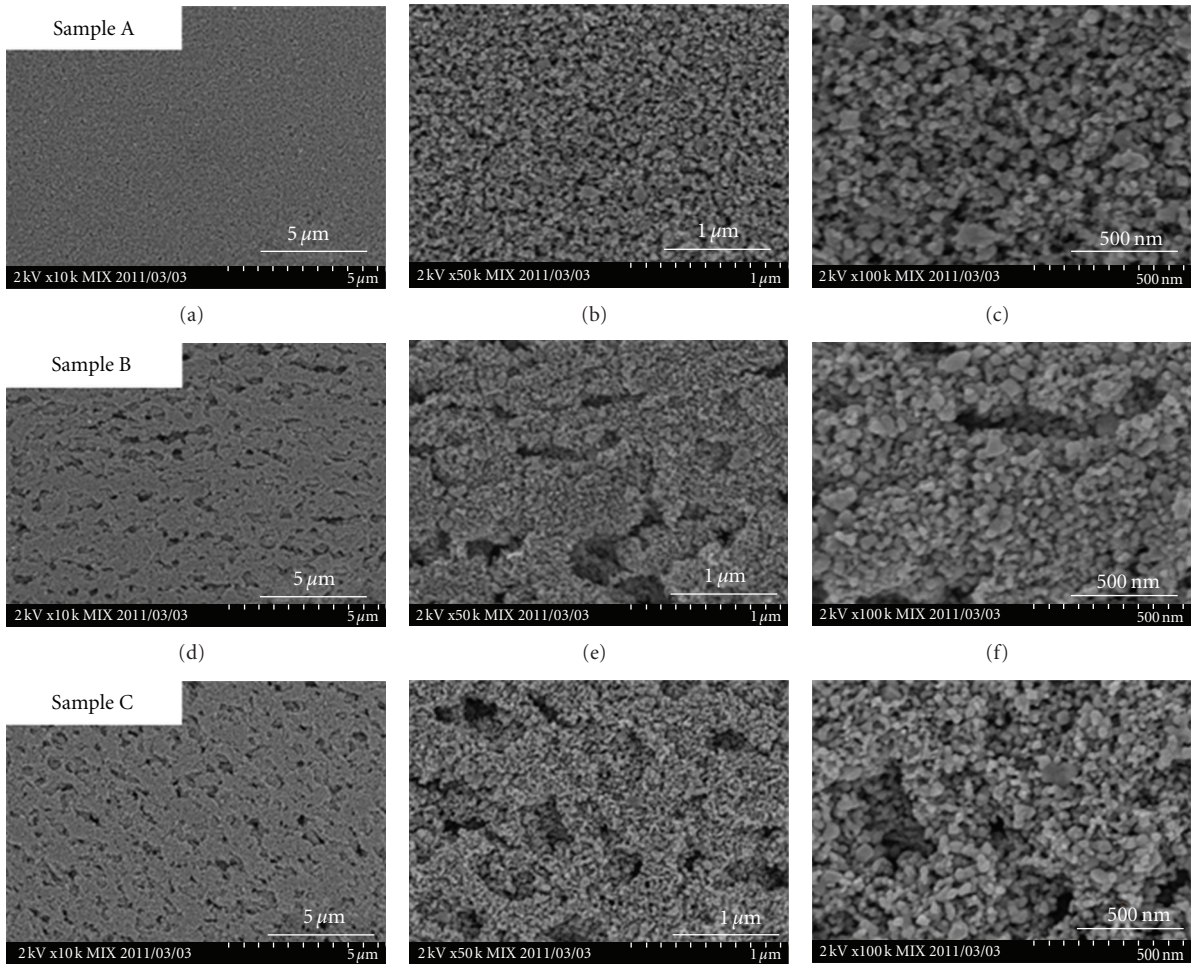

Figure 7: FE-SEM micrographs showing the surface morphology of the TiO_2 layers. The mean particle size of samples A, B, and C were 42.4, 56.9, and 73.4 nm, respectively.

Table 1: PV properties of DSSCs prepared from TiO_2 dispersions.

	Sample A	Sample B	Sample C	Sample A + Sample C
J_{SC} (mA/cm^2)	9.04	8.98	9.05	10.23
V_{OC} (V)	0.77	0.77	0.76	0.75
FF	0.67	0.68	0.67	0.67
Conversion efficiency (%)	4.65	4.72	4.64	5.17
Thickness (μm)	15.2	14.0	14.2	14.1

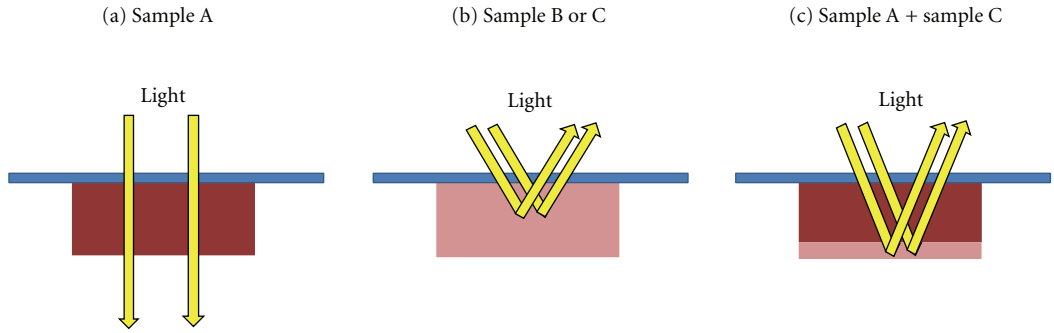

Figure 8: Schematic diagrams illustrating the effective use of incident light.

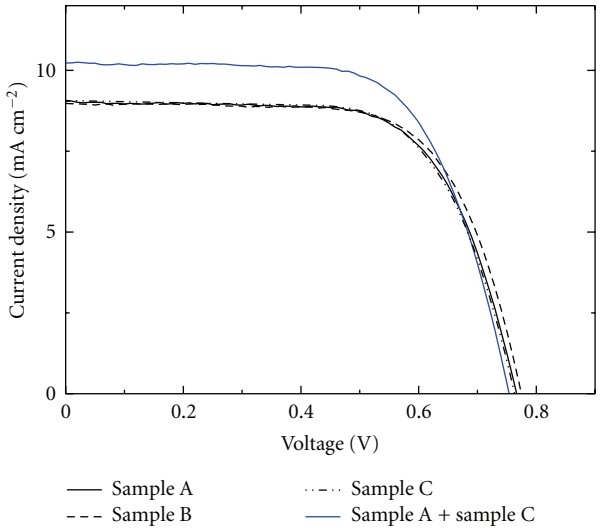

Figure 9: *I-V* characteristics of DSSCs with TiO_2-coated layer made from samples A–C.

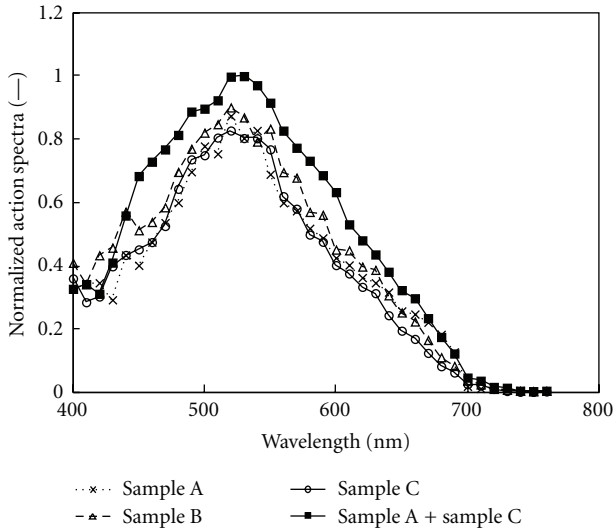

Figure 10: Photo action spectra of dye-sensitized solar cells, which were normalized to the peak of sample A + C.

the layer without absorption (Figure 8(a)). However, the transparencies of samples B and C were low, so that incident light cannot be effectively used (Figure 8(b)). If incident light is effectively absorbed in the transparent nanocrystalline-TiO_2 electrode (Figure 8(a)), high conversion efficiency can be expected. In order to effectively absorb the incident light, samples A and C were combined in consideration of the light-scattering effects. The incident light is scattered or reflected in the layer of sample C after passing through a layer of sample A, and reflected light passes through the layer of sample A again, as shown in Figure 8(c). Figure 9 shows *I-V* curves for DSSCs with coated layers of sample A, B, C, and A + C (double layer, Figure 8(c)). The A + C double layer has higher conversion efficiency than the single-layer DSSCs. The short-circuit density was increased to 1.2 mA/cm^2 and the PV conversion efficiency was improved by 10.1% using the double layer. Therefore, the characteristics of the layer structures can be controlled by changing the size distribution of TiO_2 aggregation in the layer, and the conversion efficiency can be improved easily improved by optimization of the PV characteristics.

Figure 10 shows normalized action spectra. Each cell shows the maximum value around 520 nm. However, it was confirmed that the action spectra differed by the wavelength; in spite of the similar response in the blue light region (400–430 nm), the action spectrum of A + C double layer was

improved in the longer wavelength more than 440 nm. Then, the A + C double layer has higher the value of short-circuit photocurrent density than that of the single layer.

4. Conclusions

TiO_2 powder was dispersed by the bead-milling method, and the dispersivity of TiO_2 was controlled by changing the solvent blend ratio of ethanol and terpineol in the dispersion. The coated layer became significantly opaque due to light scattering when particles greater than 100 nm were present in the coated layer, although the resulting PV effects were very similar, regardless of the mean particle size of TiO_2 aggregations in the dispersion. A double-layer structure was adopted to improve the PV effect, and the photocurrent and conversion efficiency were successfully improved.

References

[1] B. O'Regan and M. Grätzel, "A low-cost, high-efficiency solar cell based on dye-sensitized colloidal TiO_2 films," *Nature*, vol. 353, no. 6346, pp. 737–740, 1991.

[2] R. Soda, J. Kano, and F. Saito, "Analysis of effect of pin configuration on beads motion in a stirred mill by DEM," *Journal of the Society of Powder Technology*, vol. 46, pp. 180–186, 2009.

[3] M. Fujimoto, T. Kado, W. Takashima, K. Kaneto, and S. Hayase, "Dye-sensitized solar cells fabricated by electrospray coating using TiO_2 nanocrystal dispersion solution," *Journal of the Electrochemical Society*, vol. 153, no. 5, pp. A826–A829, 2006.

[4] P. M. Sirimanne, M. K. I. Senevirathna, E. Premalal, P. K. D. D. P. Pitigala, V. Sivakumar, and K. Tennakone, "Utilization of natural pigment extracted from pomegranate fruits as sensitizer in solid-state solar cells," *Journal of Photochemistry and Photobiology A*, vol. 177, no. 2-3, pp. 324–327, 2006.

[5] X. H. Zhang, C. Li, W. B. Wang, X. X. Cheng, X. S. Wang, and B. W. Zhang, "Photophysical, electrochemical, and photoelectrochemical properties of new azulene-based dye molecules," *Journal of Materials Chemistry*, vol. 17, no. 7, pp. 642–649, 2007.

[6] S. R. Jang, C. Lee, H. Choi et al., "Oligophenylenevinylene-functionalized Ru(II)-bipyridine sensitizers for efficient dye-sensitized nanocrystalline TiO_2 solar cells," *Chemistry of Materials*, vol. 18, no. 23, pp. 5604–5608, 2006.

[7] J. Yu, J. Fan, and L. Zhao, "Dye-sensitized solar cells based on hollow anatase TiO_2 spheres prepared by self-transformation method," *Electrochimica Acta*, vol. 55, no. 3, pp. 597–602, 2010.

[8] S. Ito, K. Ishikawa, C. J. Wen, S. Yoshida, and T. Watanabe, "Dye-sensitized photocells with meso-macroporous TiO_2 film electrodes," *Bulletin of the Chemical Society of Japan*, vol. 73, no. 11, pp. 2609–2614, 2000.

[9] Y. J. Kim, M. H. Lee, H. J. Kim et al., "Formation of highly efficient dye-sensitized solar cells by hierarchical pore generation with nanoporous TiO_2 spheres," *Advanced Materials*, vol. 21, no. 36, pp. 3668–3673+3618, 2009.

[10] S. Ito, S. Yoshida, and T. Watanabe, "Fabrication and characterization of meso-macroporous anatase TiO_2 films," *Bulletin of the Chemical Society of Japan*, vol. 73, no. 8, pp. 1933–1938, 2000.

[11] M. Kiyono, *Sanka Titan*, Gihodo shuppan, Tokyo, Japan, 1991.

[12] W. Jaenick, *Zeitschrift für Elektrochemie*, vol. 60, p. 163, 1956.

[13] H. H. Weber and J. Gerhards, *Farbe und Lack*, vol. 67, p. 434, 1961.

[14] P. B. Mitton,*Official Digest*, vol. 34, p. 73, 1962.

[15] F. B. Stieg, "Latex paint opacity—a complex effect," *Journal Oil Colour Chemists Association*, vol. 53, p. 469, 1970.

[16] S. Hore, P. Nitz, C. Vetter, C. Prahl, M. Niggemann, and R. Kern, "Scattering spherical voids in nanocrystalline TiO_2—enhancement of efficiency in dye-sensitized solar cells," *Chemical Communications*, no. 15, pp. 2011–2013, 2005.